Climate Dynamics (2020) 54:3991–4004
https://doi.org/10.1007/s00382-020-05217-2

A global analysis of austral summer ocean wave variability during SAM–ENSO phase combinations

Victor A. Godoi[1] · **Audalio R. Torres Júnior**[1]

Received: 28 October 2019 / Accepted: 13 March 2020 / Published online: 25 March 2020

Abstract
Anticipating and mitigating wave-related hazards rely heavily on understanding wave variability drivers. Here, we describe wave conditions related to concurrent Southern Annular Mode (SAM) and El Niño–Southern Oscillation (ENSO) phases during the austral summer. To identify such conditions, significant wave height (H_s) and peak wave period (T_p) daily anomalies were composited during different SAM–ENSO phase combinations over the last four decades (1979–2018). Surface wind anomalies were also composited to assist in the interpretation of wave conditions. The composites show significant wave variability across all ocean basins and in several semi-enclosed seas throughout the different SAM–ENSO phase combinations. The Southern, Indian, and Pacific Oceans generally experience the strongest T_p anomalies during combinations of SAM phases with El Niño, and the weakest T_p anomalies during combinations of SAM phases with La Niña. The anomalously large waves observed in the south-western Pacific, Tasman Sea, and the Southern Ocean, previously ascribed to ENSO conditions, seem to be instead associated with the SAM variability. SAM-related atmospheric conditions are found to be able to modulate the intensity of ENSO-related winds over the South China Sea, which, in turn, alter the magnitude of waves in that region. These and other wave anomaly structures described here, especially those contrasting the behaviour expected for a given ENSO phase, such as the one found along the California coast, stress the importance of understanding relationships between wave parameters and climate patterns interactions.

Keywords Climate patterns · El Niño–Southern Oscillation (ENSO) · Global wave climate · Southern Annular Mode (SAM) · SAM–ENSO interactions · Wave variability

1 Introduction

Ocean surface gravity waves (henceforth waves) threat the safety of coastal and offshore infrastructures and pose a substantial risk to people living and working near and on the ocean. Anticipating and mitigating wave-related hazards require an in-depth understanding of wave variability drivers at several timescales. Such drivers are relatively well understood at short timescales (of up to a few days). At longer timescales, nevertheless, the wave variability resulting from the complex atmospheric and oceanic conditions associated with climate patterns and their interactions make coastal hazard risk management and adaptation planning challenging.

Previous work ascribed wave variability at intra-seasonal or longer timescales mostly to individual climate patterns (e.g., Stopa et al. 2013; Reguero et al. 2015; Godoi et al. 2016). By disregarding relationships with the co-occurrence of multiple climate patterns, these studies camouflage the actual wave variability drivers (Godoi et al. 2019, 2020). For instance, during periods when El Niño co-exists with active Madden–Julian Oscillation (MJO—Madden and Julian 1971, 1972, 1994), the anomalously large waves that generally impact the California coast as a result of El Niño-related conditions (Barnard et al. 2015, 2017) only take place during two out of the eight MJO phases (Godoi et al. 2020). In other words, most MJO-related conditions suppress wave increases in that region when coinciding with El Niño episodes. Another interesting example of changes in the expected wave conditions is the sign reversal of wave anomalies in the South China Sea during the co-occurrence

✉ Victor A. Godoi
victorgodoirj@gmail.com

[1] Marine Science Institute (ICMar), Federal University of Maranhão, Av. dos Portugueses, 1966, São Luís 65080-805, Brazil

of La Niña with MJO phase 3 (Godoi et al. 2020). Wave height anomalies are usually positive (waves get larger than typical waves) in the South China Sea during La Niña (Zhu et al. 2015). However, when the latter combines with MJO phase 3, wave anomalies not only weaken but also become negative (waves get smaller than typical waves) (Godoi et al. 2020). Therefore, it is essential to understand changes in wave conditions during the co-existence of multiple climate patterns so that coastal planners can develop more reliable management plans. Two climate patterns are of particular interest because of their already-verified strong interactions, the Southern Annular Mode (SAM—Limpasuvan and Hartmann 1999) and the El Niño–Southern Oscillation (ENSO—Walker and Bliss 1932, 1937; Philander 1983; Neelin et al. 1998).

The SAM, or Antarctic Oscillation (Gong and Wang 1999), is the dominant pattern of large-scale atmospheric variability in the extratropical Southern Hemisphere (Marshall 2003), whose timescales range from intra-seasonal to inter-annual (Vera and Osman 2018). The SAM is associated with atmospheric mass exchanges between the mid and high latitudes (Simmonds and King 2004), which result in a zonally-symmetric structure (Gong and Wang 1999) that can be identified year-round (Thompson and Wallace 2000) in several atmospheric fields, such as geopotential height and sea-level pressure (Rogers and van Loon 1982). The positive SAM phase is defined by above-normal mean sea-level pressure (MSLP) in mid latitudes and below-normal MSLP in high latitudes (Wang and Cai 2013), accompanied mainly by the strengthening of the westerly winds that encircle Antarctic (Rogers and van Loon 1982) and by a poleward movement of this belt (Goodwin 2005). The opposite pattern characterises the negative SAM phase.

The ENSO is an inter-annual oscillation whose signals prevail in the 2–7 years range (Trenberth and Hurrell 1994; Cane 2005). Its associated effects occur all over the world and affect, for instance, agriculture and freshwater supply (Collins et al. 2010). The ENSO's main signature manifests in the central and eastern tropical Pacific as sea surface temperature (SST) anomalies, with persisting colder-than-normal waters defining a La Niña episode and warmer-than-normal waters an El Niño episode (Chase et al. 2006). Under normal conditions (inactive ENSO), trade winds over the Pacific basin push the surface warm water westward and pile it up near Indonesia. The accumulated water pushes the thermocline down, while it rises in the eastern Pacific bringing cold water up to the surface. During La Niña, strengthened trade winds reinforce the "normal conditions", and the typical eastern tropical Pacific upwelling enhances. During El Niño, the trade winds weaken, and reverse direction occasionally, facilitating the surface warm water eastward movement from the western to the central and eastern Pacific. Enhanced atmospheric convection develops over the regions where anomalous warm waters take place during both El Niño and La Niña, and this influences weather patterns dynamics worldwide.

Areas far beyond the regions where the SAM and ENSO are most pronounced can experience their signals via teleconnection mechanisms—Liu and Alexander (2007) defined teleconnection as "the linkage of seemingly unrelated climate anomalies over great distances". Several mechanisms have been proposed to explain how climate patterns prevailing in a given region may be related to remote anomalies in the ocean and atmosphere; these include, for example, an "atmospheric bridge" (e.g., Alexander et al. 2002), wave trains (e.g., Mo and Paegle 2001; Yang et al. 2018), an eddy-jet stream mechanism (e.g., Yang et al. 2018), and a stratospheric pathway mechanism (e.g., Mechoso et al. 1985; Hurwits et al. 2011). Explanations of teleconnection mechanisms generally involve changes in the fluxes of momentum, heat, and moisture associated with the atmospheric Walker and Hadley circulations. The Walker circulation links two remote tropical areas (tropic–tropic teleconnections), whereas the Hadley circulation links a tropical area to a subtropical one, where Rossby wave sources disturb extratropical atmospheric and oceanic phenomena through such waves (tropic–extratropic teleconnections) (Grimm and Ambrizzi 2009; Shimizu and Cavalcanti 2011). Mid-latitude excitations of tropical waves can also occur (e.g., Hoskins and Yang 2000), as part of the two-way tropic–extratropic interaction (e.g., MacRitchie and Roundy 2016), as well as inter-hemispheric teleconnections (e.g., Nan and Li 2003; Wu et al. 2009; Sun 2010; Mamalakis et al. 2018). Furthermore, the signals of a given climate pattern can propagate to distant regions through another climate pattern (e.g., Klein et al. 1999). A large body of literature describing teleconnection mechanisms is available (e.g., Bjerknes 1969; Karoly 1989; Mo 2000; Alexander et al. 2002; Turner 2004; L'Heureux and Thompson 2006; Liu and Alexander 2007; Sun et al. 2010; Cai et al. 2011a, b; Ding et al. 2012, 2014; Liu et al. 2015, 2018; Rudeva and Simmonds 2015; Yu et al. 2015; Feldstein and Franzke 2017; Stan et al. 2017; Yang et al. 2018), and so the reader is referred to the studies cited in this paragraph for detailed information on this topic. Regarding SAM–ENSO interactions, the ENSO teleconnection to Southern Hemisphere high-latitudes, especially to the South Pacific (Carleton 2003), has been found to be favoured during co-occurrences of La Niña with positive SAM, and El Niño with negative SAM (Carvalho et al. 2005; Fogt and Bromwich 2006; Stammerjohn et al. 2008; Fogt et al. 2011). These co-occurrences correlate more strongly during the austral summer (Fogt et al. 2011). The type of ENSO also appears to play an important role in exciting the SAM; the central Pacific type exerts a significant impact on the SAM, whereas the eastern Pacific type does not (Yu et al. 2015).

Local, regional, hemispheric, and global wave conditions have been related to the SAM (e.g., Harley et al. 2010; Hemer 2010; Hemer et al. 2010; Godoi et al. 2016, 2018; Marshall et al. 2018). Changes in wave conditions associated with ENSO phase shifts have also been vastly explored at several spatial scales (e.g., Harley et al. 2010; Hemer et al. 2010; Izaguirre et al. 2011; Shimura et al. 2013; Stopa et al. 2013; Stopa and Cheung 2014; Godoi et al. 2016, 2018). Nevertheless, the way global waves behave under intense activity of simultaneous SAM and ENSO phases has not yet been investigated. This knowledge gap has been filled here by analysing the variability of wave parameters during the austral summer (December–February), when ENSO reaches its mature stage (Philander 1983; Carvalho et al. 2005) and interactions between the SAM and ENSO are most favoured (Lim et al. 2013). As noted by Marshall et al. (2018), who examined the association of global wave variability with SAM phases, changes in wave conditions have little influence from SAM–ENSO interactions during seasons other than summer. The authors verified this by comparing, for each season, wave anomaly composites calculated for two sets of periods of active SAM, one that included both active ENSO and ENSO–neutral episodes and the other that included only ENSO–neutral years. Marshall et al. (2018), however, did not distinguish between La Niña and El Niño events when considering active ENSO phases. As shown later in this paper, this distinction is of paramount importance to thoroughly understand global wave anomalies during simultaneous summertime SAM–ENSO events. We investigated wave variability through composites of daily anomalies in wave parameters calculated for different SAM–ENSO phase combinations over the period 1979–2018.

The data and methods used in this research are described in the following section. Section 3 presents the results obtained and discusses the differences in wave variability among the different SAM–ENSO phase combinations. Lastly, the conclusions are documented in Sect. 4.

2 Data and methods

Hourly significant wave height (H_s) and peak wave period (T_p) fields, at the spatial resolution of 0.4°, were obtained from the Centre for Australian Weather and Climate Research (CAWCR) long-term global wave hindcast (Durrant et al. 2013a, b, 2014). This hindcast was carried out using versions 4.08 (for the period January 1979–May 2013—Durrant et al. 2014) and 4.18 (from June 2013 onwards—Hemer et al. 2017) of the spectral wave model WAVEWATCH III (WW3—Tolman 1991, 2014). The model was forced with hourly 10 m wind and six-hourly sea ice concentration data from the National Oceanic and Atmospheric Administration (NOAA) National Centers for Environmental Prediction (NCEP) Climate Forecast System (CFS) Reanalysis (CFSR) dataset (Saha et al. 2010) (sourced for the period January 1979–December 2010) and its extension NOAA NCEP CFS version 2 (CFSv2) dataset (Saha et al. 2014) (sourced for January 2011 onwards). These wind data were also used here to assist in the interpretation of the wave anomalies observed during SAM–ENSO phase combinations. Details on the hindcast simulation and its validation can be found in Durrant et al. (2014) and Hemer et al. (2017).

Inhomogeneities in the reanalysed winds due to changes in the amount of data assimilated by the CSFR atmospheric model and to spatial resolution upgrade (CFSR: ~0.3°; CFSv2: ~0.2°) are discussed in Chawla et al. (2013), Stopa et al. (2013), and Stopa (2018). Although these inhomogeneities are recognised, it is unlikely that they influence the results of this work significantly because (1) temporally-averaged wave anomalies have been used; (2) the focus of this study is on the spatial patterns of wave anomalies, rather than on their absolute values; (3) trends in wave parameters have not been analysed. The potential inhomogeneity related to the WW3 upgrade from version 4.08 to 4.18 is believed to be only minor (if existent indeed), since there were no changes in the model physics employed (Hemer et al. 2017).

NOAA Climate Prediction Center (CPC) Oceanic Niño Index (ONI) (L'Heureux et al. 2013) and daily AAO index (referred to here as SAM index) (Ho et al. 2012) were used to determine ENSO and SAM phases, respectively. ONI values (3-month running means of SST anomalies in the Niño 3.4 region) remaining above 0.5 °C and below −0.5 °C for at least five consecutive overlapping seasons were defined as El Niños and La Niñas, respectively. Following Marshall et al. (2018), positive and negative SAM phases (+SAM and −SAM) were defined by SAM index values higher and lower than one standard deviation (σ) about the mean (μ), respectively; i.e., $+\text{SAM} > \mu + 1\sigma$ and $-\text{SAM} < \mu - 1\sigma$. To match the SAM index temporal resolution, the ONI value of a given month was assigned to all days of that month.

Daily anomalies in H_s, T_p, and wind fields were composited (temporally averaged) over all days comprised by each SAM–ENSO phase combination during the austral summer over the period 1979–2018. Significance of the composites was verified using a two-tailed Student's t test (Student 1908), considering the 95% confidence level and the effective number of spatial degrees of freedom (N_{eff}) (Bretherton et al. 1999), defined as $N_{eff} = N[(1-\rho)/(1+\rho)]$; where N is the number of days used to calculate the composite, and ρ is the lag-1 autocorrelation coefficient of the variable of interest (H_s, T_p, or wind velocity). ρ is used to ensure independence between the daily anomalies in spatial fields (Wilks 2006).

3 Results and discussion

Figures 1, 2 and 3 show wind at 10 m, H_s, and T_p composites, respectively, for SAM–ENSO phase combinations during the austral summer over the period 1979–2018. Only statistically significant results at the 95% confidence level are displayed.

A few aspects of the long-term wave climate can be noted in Fig. 2 and supported by Fig. 1. For example, to maintain the airflow through the Drake Passage, the winds strengthen (see, e.g., combinations of +SAM with active ENSO phases—upper panels of Fig. 1) and create large waves in that region (Fig. 2). As cyclones are consistently generated and propagate over the Southern Ocean, this is a very active wave generation zone (Young 1999; Sterl and Caires 2005), in which increases and decreases in wave height are highly sensitive to changes in wind velocity (see the differences in wind and H_s patterns between positive and negative SAM phases). Trade winds intensify in the central Pacific during La Niña (easterly anomalies) and weaken during El Niño (westerly anomalies) (Fig. 1). Despite the wind intensification during La Niña episodes, waves do not increase in the central Pacific

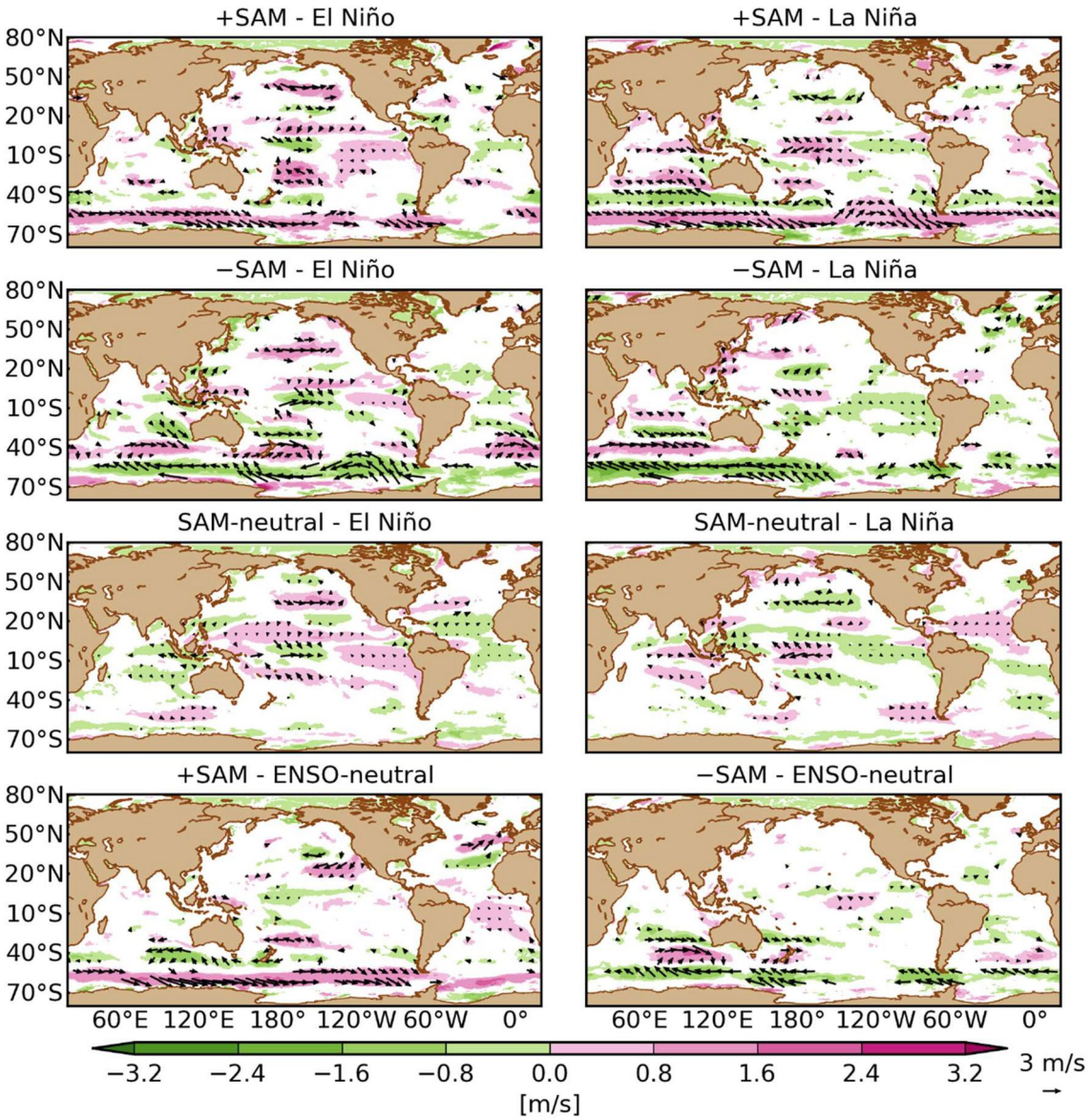

Fig. 1 Wind at 10 m daily anomaly composites for SAM–ENSO phase combinations over the austral summer (DJF) during the period 1979–2018. +SAM and −SAM stand for positive and negative SAM phases, respectively. Only statistically significant anomalies at the 95% confidence level are displayed

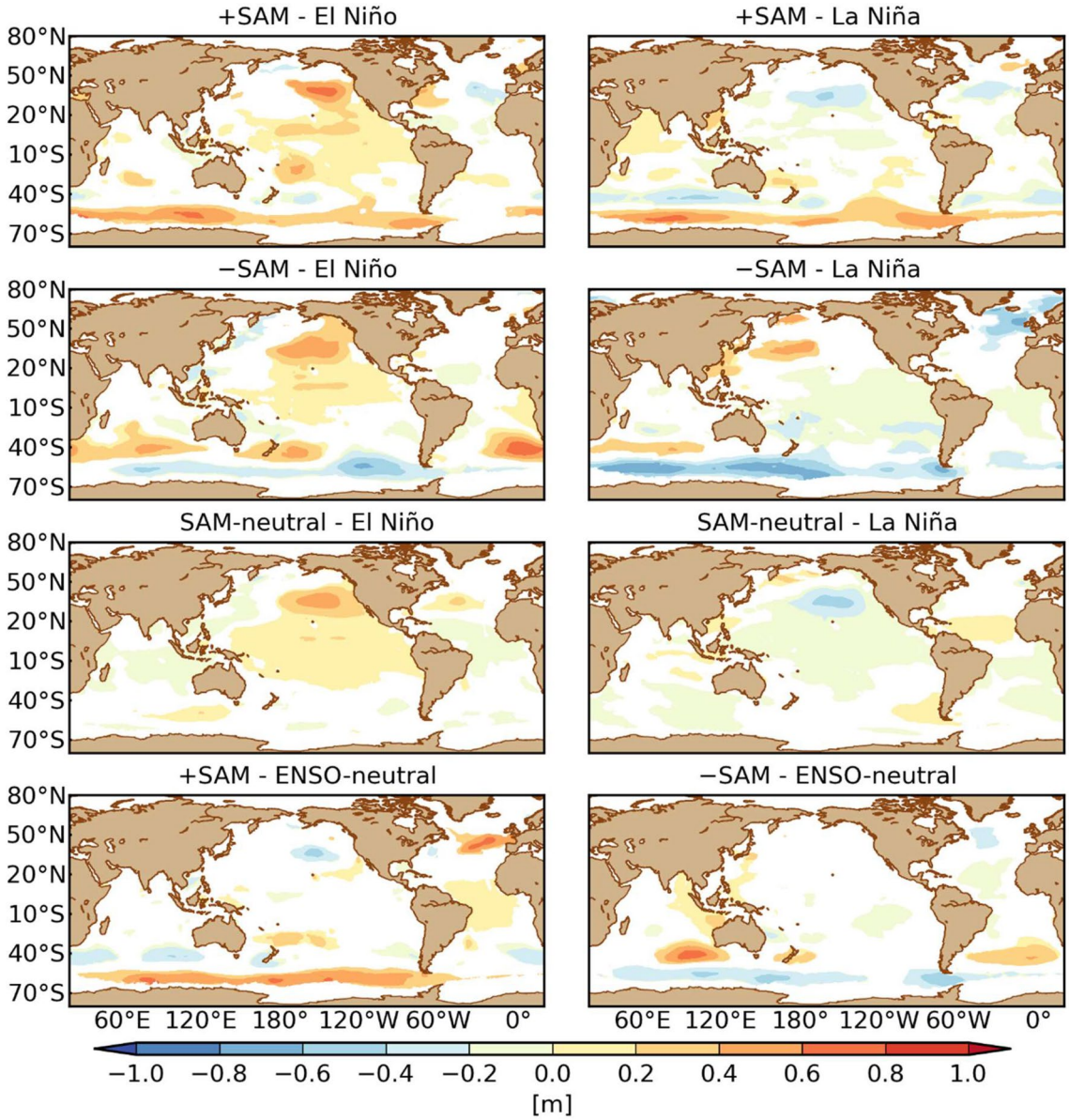

Fig. 2 Significant wave height daily anomaly composites for SAM–ENSO phase combinations over the austral summer (DJF) during the period 1979–2018. +SAM and −SAM stand for positive and negative SAM phases, respectively. Only statistically significant anomalies at the 95% confidence level are displayed

(see combinations of SAM phases with La Niña—Fig. 2) because the wave climate of tropical latitudes is dominated by swells (Young 1999; Chen et al. 2002; Semedo et al. 2011), i.e., remotely-generated waves that can propagate over long distances after leaving their generation zones. Although La Niña-related stronger winds can generate larger wind-seas, i.e., waves within the generation zone that are still growing and developing longer periods as a result of the wind action, the overall spectral energy is still dominated by swells. Thus, the energy of wind-seas does not contribute to H_s (average of the highest one-third of waves that occur in a given time interval) in the central Pacific during combinations of SAM phases with La Niña.

The main signatures of both the SAM and ENSO are remarkably present in the wind and H_s composites (Figs. 1, 2). Irrespective of the ENSO phase, combinations with +SAM are associated with larger waves in the Southern Ocean (Fig. 2) as a result of stronger mid- to high-latitude westerlies (Fig. 1). These wave anomalies are less evident in the Atlantic sector of the Southern Ocean, due likely to the shadowing caused by the South American landmass, which blocks the propagation of swell from the Pacific sector

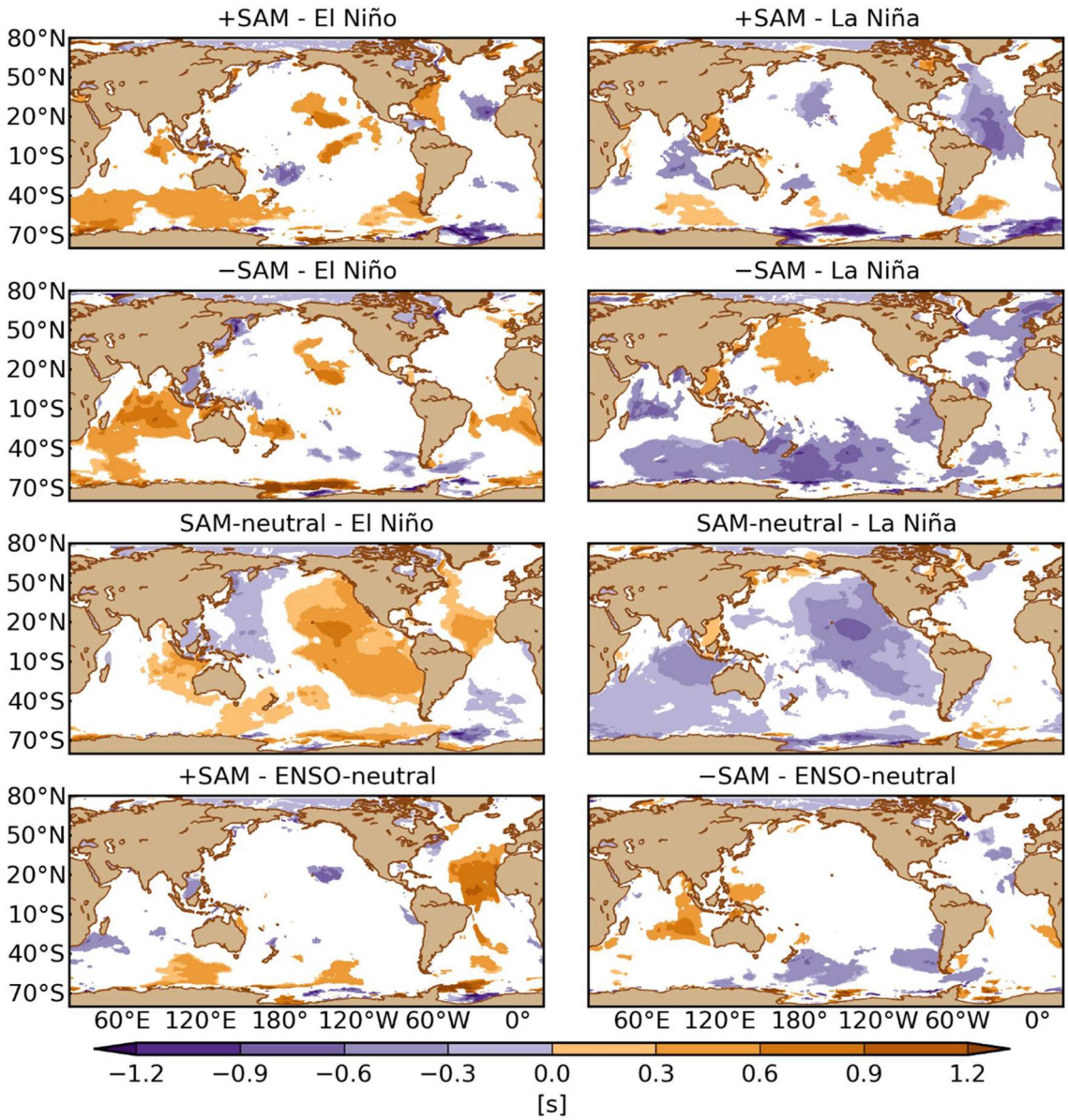

Fig. 3 Peak wave period daily anomaly composites for SAM–ENSO phase combinations over the austral summer (DJF) during the period 1979–2018. +SAM and −SAM stand for positive and negative SAM phases, respectively. Only statistically significant anomalies at the 95% confidence level are displayed

(Hemer et al. 2010). Conversely, weaker mid- to high-latitude westerlies over the Southern Ocean (represented by easterly anomalies with negative speed—Fig. 1) lead to smaller waves in the same region when −SAM combines with ENSO phases (Fig. 2). In the same ocean, anomalies in H_s have only small magnitudes during the SAM neutral phase, indicating the SAM dominance in the Southern Hemisphere storm track region (30–60° S). The dominance of ENSO in the tropical and central North Pacific manifests through larger waves during El Niño and smaller waves during La Niña, regardless of the SAM phase (Fig. 2). The most notable feature, in this case, is the blob of positive H_s anomalies to the north of Hawaii that appears during combinations of SAM phases with El Niño. This blob varies in size and strength depending on the SAM phase, being most pronounced during +SAM–El Niño (anomalies of up to 0.8 m). The associated wind anomalies are predominantly from the west (Fig. 1).

In general, T_p anomalies in the Southern, Indian, and Pacific Oceans are strongest during combinations of SAM phases with El Niño (+SAM–El Niño, −SAM–El Niño, and SAM–neutral–El Niño, respectively—Fig. 3). The Atlantic Ocean, on the other hand, experiences the strongest T_p anomalies during +SAM–ENSO–neutral. Shorter-period

waves cover large portions of the Southern, Indian, Pacific, and Atlantic Oceans during combinations of SAM phases with La Niña (−SAM–La Niña, SAM–neutral–La Niña, SAM–neutral–La Niña, and +SAM–La Niña, respectively). Therefore, the overall picture of T_p anomalies in the main ocean basins during SAM–ENSO phase combinations suggests these anomalies are mostly driven by ENSO-related conditions. Waves generated in the Southern Ocean have long been known to propagate across the Pacific and, consequently, impact coasts in Central and North America (Munk and Snodgrass 1957; Munk et al. 1963; Snodgrass et al. 1966; Young 1999). Despite this, positive T_p anomalies generated by the stronger winds that blow over the Southern Ocean during +SAM–ENSO–neutral (Fig. 1) are confined to that ocean (Fig. 3). This result does not mean that longer-period waves do not propagate across the Pacific Ocean during +SAM–ENSO–neutral, it only means that, on average, they are not statistically significant. Durrant et al. (2014) mentioned that the sheltering coefficient of Ardhuin et al. (2010) source terms was adjusted when producing the hindcast data used here to minimise the positive bias in H_s found in the Southern Ocean in comparisons to measured data. Such adjustment affects the shorter-period waves generated under high wind speed conditions and, therefore, should not affect the longer-period waves under question. Other interesting characteristics of the T_p anomaly composites can be enumerated as follows: (1) T_p anomalies in the central and eastern Pacific are almost mirrored during combinations of SAM–neutral with opposite ENSO phases (see 3rd row of Fig. 3); (2) −SAM-related conditions strengthen the T_p anomalies that appear in the South China Sea during combinations of SAM–neutral with active ENSO phases (compare the panels in the 2nd row of Fig. 3 to those in the 3rd row); (3) Although negative T_p anomalies appear in the South China Sea during +SAM–ENSO–neutral, conditions associated with active ENSO phases dominate that region. Such conditions make T_p anomalies disappear during +SAM–El Niño and reverse their sign during +SAM–La Niña; (4) Negative T_p anomalies appear all over the Sea of Japan during –SAM–El Niño, whereas positive anomalies are experienced in its southern portion during –SAM–La Niña.

As expected, H_s and T_p composites for combinations of SAM phases with ENSO–neutral (Figs. 2 and 3, respectively) resemble those of Marshall et al. (2018) in which the authors excluded active ENSO years from their calculations (as previously mentioned, Marshall et al. (2018) analysed relationships between wave variability and SAM phases). Since we used the same wave hindcast data as Marshall et al. (2018), the differences in the composites can be attributed to the longer period analysed here (1979–2018) relative to that (1979–2009) considered by Marshall et al. (2018), meaning that the present analysis covers more +SAM/−SAM–ENSO–neutral events. For +SAM–ENSO–neutral combinations, the most noteworthy differences between the two studies are the presence of negative H_s anomalies off north-western Australia and in the south-western Atlantic, most noticeable in Marshall et al. (2018), and of the strip of positive H_s anomalies between Hawaii and Baja California, observed here. Regarding T_p, positive anomalies in the central South Atlantic and negative anomalies in the central Pacific and the South China Sea are most apparent in the present work. In terms of –SAM–ENSO–neutral, the larger waves that appear in the eastern Indian Ocean in Fig. 2, from the Bay of Bengal to north-western Australia, and those occurring to the south of Japan and in the Philippine Sea are not seen in the corresponding composite of Marshall et al. (2018). Moreover, Fig. 2 shows positive H_s anomalies in the southern South Atlantic that cover a considerably wider area than those observed in the composite of Marshall et al. (2018). On the other hand, negative H_s anomalies in their composite have greater absolute magnitude (are more negative) and occupy larger areas of the North Atlantic, eastern Pacific, and the Southern Ocean, especially close to South America. Similar characteristics define the differences in T_p anomaly patterns between Fig. 3 and the corresponding composite of Marshall et al. (2018) for –SAM–ENSO–neutral, except for (1) the positive anomalies in the southern South Atlantic (as in Fig. 2), absent in both studies; (2) the longer-period waves around the south-western coast of Africa and the shorter-period waves in the south-western Pacific, observed in Fig. 3 and absent in the composite of Marshall et al. (2018); and (3) the longer-period waves off the Japanese coast, absent in Fig. 3 and present in the composite of Marshall et al. (2018).

In the Pacific basin, SAM–ENSO interactions are associated with striking features in the extratropical latitude band of both hemispheres. The anomalously large waves expected to occur along the California coast during El Niño events (Barnard et al. 2015, 2017—also noted in the SAM–neutral–El Niño composite of Fig. 2) do not appear when the SAM is active. The stretch of coastline free from the impact of larger waves during active SAM shows this feature to be noticeable during −SAM more than +SAM (compare –SAM–El Niño to +SAM–El Niño in Fig. 2). In the Southern Hemisphere, a −SAM background seems to be requisite for the generation of the larger waves that typically impact New Zealand coasts during El Niño years. This link with El Niño conditions was reported in previous work (e.g., Gorman et al. 2003; Godoi et al. 2016), which showed that larger waves occur all around New Zealand, except in the waters off the northern coastline. Surprisingly, these waves appear even in the absence of El Niño (−SAM–ENSO–neutral—Fig. 2), suggesting that they are related to wind conditions associated with −SAM more than to those associated with El Niño. The wind composites (Fig. 1) confirm this is indeed the case. South-westerly winds are anomalously strong around New

Zealand during –SAM–ENSO–neutral. Under an El Niño background (−SAM–El Niño), these winds strengthen even more and act over a much broader area. On the other hand, wind anomalies are almost negligible around New Zealand when the SAM is in the neutral phase and El Niño is taking place. In these circumstances, the existing wind anomalies are negative and cover only a small area off the eastern coast. This is reflected in the corresponding H_s composite (Fig. 2), which shows a similar anomaly spatial pattern. Another aspect that corroborates the assumption that wave anomalies around New Zealand are related to the SAM more than to ENSO is their sign reversal during +SAM relative to −SAM for the same ENSO phase (El Niño)—wave anomalies become negative during +SAM–El Niño. The analysis of wave anomalies during combinations of SAM phases with La Niña episodes reinforces this assumption once more. Previous work states that waves are expected to increase to the north of New Zealand during La Niña episodes (Gorman et al. 2003; Godoi et al. 2016). Figure 2 shows this only happens during +SAM–La Niña. The +SAM–ENSO–neutral and SAM–neutral–La Niña phase combinations reveal that the waves affecting the New Zealand northern coast are indeed generated by SAM-related wind conditions, and not by those conditions related to La Niña (Fig. 1).

By looking at tropical latitudes, one observes slightly larger waves covering a large portion of the Pacific Ocean basin during SAM–neutral–El Niño (Fig. 2), with concomitant longer periods in the eastern half (Fig. 3). The area of strongest H_s anomalies (up to 0.6 m) coincides with that of strongest wind anomalies in the central North Pacific (Fig. 1), whereas the strongest T_p anomalies are found to the south (Fig. 3), in tropical latitudes. Similar spatial patterns of H_s, wind, and T_p, but with opposite anomalies, occur during SAM–neutral–La Niña.

As storm propagation over the Southern Ocean has a particular behaviour depending on the SAM phase, so do waves. Waves generally increase in the waters off southwestern Australia during −SAM because storm tracks over the Southern Ocean are shifted northward compared to the long-term mean track (Bosserelle et al. 2012). These larger waves are the most remarkable feature of the –SAM–ENSO–neutral composite (Fig. 2); they reflect the cyclonic wind intensification over the same region (Fig. 1). Similar patterns for both wind and H_s are observed off southwestern Australia when El Niño coincides with −SAM, but, in this case, they exhibit weaker anomalies. Contrary to −SAM-related conditions, +SAM is associated with a southward displacement of cyclone tracks over the Southern Ocean (Gillett and Thompson 2003). This creates belts of stronger westerly winds (Thompson and Solomon 2002) and larger waves (Hemer et al. 2010) in that region, like the ones shown in the +SAM–ENSO–neutral composites of Figs. 1 and 2, respectively. The formation of these belts has been favoured by the trend toward more positive SAM phases (Thompson and Solomon 2002; Marshall 2003), especially in recent summers (Marshall 2003; Fogt et al. 2009). As seen for combinations of −SAM with both ENSO–neutral and El Niño, wind and H_s patterns in the Southern Ocean have similar characteristics during +SAM–ENSO–neutral and +SAM–El Niño. Under an El Niño background, nonetheless, winds strengthen and waves increase in the Indian Ocean sector of the Southern Ocean (along the "furious fifties") relative to ENSO–neutral, while the opposite happens in the Pacific Ocean sector.

Two areas have the most noteworthy anomalously large waves in the Atlantic basin, one in the Southern Hemisphere during –SAM–El Niño and the other in the Northern during +SAM–ENSO–neutral. The Southern Hemisphere one is found in the south-eastern Atlantic, and consists of waves generated locally (Fig. 2) by stronger cyclonic winds (Fig. 1). Intensification of these winds is favoured by conditions associated with both −SAM (Veitch et al. 2019) and El Niño (Colberg et al. 2004). Comparison between the wind composites for –SAM–ENSO–neutral and SAM–neutral–El Niño clearly shows the SAM dominance in wind strengthening (Fig. 1). The waves generated by these stronger winds in the south-eastern Atlantic during –SAM–El Niño impact the whole coastline of South Africa (Fig. 2), and are associated with longer periods in most parts of it (Fig. 3). These results support the findings of Veitch et al. (2019), who analysed the wave record of a location near Cape Point, on the southwestern coast of South Africa. The area encompassing the most striking larger waves in the North Atlantic extends across the northern section of this ocean, and consists of H_s anomalies that are strongest in its central portion and of sizeable magnitude in the Bay of Biscay and surrounding coasts (+SAM–ENSO–neutral—Fig. 2). These anomalies show no relationships with active ENSO phases. This independence from ENSO was recently discussed by Marshall et al. (2018), who noted in addition that teleconnections associated with active ENSO phases act to dampen SAM-related Northern Hemisphere wave anomalies. Our composites reaffirm their remark on the damping effect. On the other hand, teleconnections triggered by conditions related to simultaneously active SAM and ENSO phases may contribute to changing the spatial structure of wave anomalies relative to when the activity of only one of the patterns (either the SAM or ENSO) induces teleconnections. For instance, during +SAM–El Niño, larger waves occur in the waters adjacent to the coastline sector from southeastern Florida, in the United States, all the way up to Nova Scotia, in Canada (Fig. 2). In this case, +SAM-related and El Niño-related anomalies are neither intensified nor dampened during +SAM–El Niño. When combined, +SAM and El Niño lead to a distinct anomaly spatial structure (compare H_s anomalies in that area during +SAM–El Niño to those

during both +SAM–ENSO–neutral and SAM–neutral–El Niño). The longer wave periods associated with such anomalous waves along the United States eastern seaboard increase the likelihood of more severe damage to coastal infrastructure (Fig. 3). These notable anomalies in H_s and T_p do not appear in the composites of Marshall et al. (2018) because El Niño and La Niña episodes are not treated separately in their analysis. This difference between the present work and that of Marshall et al. (2018) reinforces a comment made in the introduction, which states that the distinction between La Niña and El Niño events is necessary for a thorough understanding of wave anomalies during periods in which the SAM and ENSO share anomalous activity. Although not considered part of the Atlantic, the North Sea can be strongly influenced by the winds that blow over this ocean and eventually traverse the United Kingdom, as is the case during +SAM–El Niño (Fig. 1), when the North Sea experiences larger and longer-period waves (Figs. 2, 3). It is also worth mentioning that weaker winds off the United Kingdom's Atlantic coasts (Fig. 1) produce smaller waves with shorter periods that arrive at the coastline during –SAM–La Niña (Figs. 2, 3). At least during the periods in which this phase combination takes place, such wave conditions will contribute to lessening the multi-hazard effects resulting from waves superimposed to extreme sea-level increases projected for that area (Vousdoukas et al. 2017).

Wave anomaly patterns in the Indian Ocean are not as prominent as those observed in the other ocean basins. During –SAM–ENSO–neutral, longer wave periods in the eastern Indian Ocean (Fig. 3) indicate that these waves are generated by remote sources. The corresponding wind composite shows a cyclonic circulation off south-western Australia (Fig. 1), which seems to be responsible for generating the swells that propagate into the eastern Indian Ocean and those that arrive in the Bay of Bengal (Fig. 2). Also during –SAM–ENSO–neutral, local wind sources (Fig. 1) increase the waves in the Andaman and Timor Seas, with H_s anomalies reaching 0.4 m in the latter (Fig. 2). Those larger waves in the Timor Sea are likely associated with the more intense activity of tropical cyclones in north-western Australia, typical of the summer season (McBride and Keenan 1982; Dare and Davidson 2004). These results, however, disagree with those of Kumar et al. (2019), who reported increases in H_s in that area during +SAM, rather than −SAM. When La Niña combines with SAM–neutral, local wind sources have a stronger effect along the equatorial Indian Ocean (Fig. 1), where stronger westerly winds generate slightly larger windseas that impact the Indonesian coast (Fig. 2). As the Indonesian landmass does not block these winds (Fig. 1), they are also capable of generating slightly larger waves with longer periods in the Java Sea (Figs. 2, 3). Positive small-amplitude H_s anomalies cover a large area of the north-western Indian Ocean and the Arabian Sea during +SAM–La Niña (Fig. 2).

When examining the Gulf of Mexico and the Caribbean and South China Seas, interesting wave patterns can also be noted. Opposite wave anomalies appear in the eastern portion of the Gulf of Mexico during SAM–neutral–El Niño and +SAM–ENSO–neutral (Fig. 2), demonstrating the teleconnecting nature of both the SAM and ENSO. Further evidencing the capability of the SAM teleconnection in changing wave conditions in that area are the slight but statistically significant differences in the wave anomaly pattern between SAM–neutral–El Niño and –SAM–El Niño. In the Caribbean Sea, wave anomalies are inexistent during combinations of active SAM with ENSO–neutral (Figs. 2, 3). Marshall et al. (2018) obtained the same results, not only for these specific phase combinations but also for those considering active ENSO. Here, in contrast, H_s anomalies of opposite signs occur in the Caribbean Sea during +SAM–El Niño and +SAM–La Niña (Fig. 2) as a consequence of opposite local wind anomalies (Fig. 1). By comparing these composites to those for SAM–neutral–El Niño and SAM–neutral–La Niña, it is possible to identify some significant differences. Although anomalies in the Caribbean Sea during combinations with +SAM result primarily from conditions associated with active ENSO phases, the +SAM-related teleconnection does seem to play a role in that region, since wind and H_s anomalies are observed at different locations relative to those generated during SAM–neutral. The difference in location of the wave anomalies between +SAM–El Niño and SAM–neutral–El Niño is considerably more evident for T_p, with shorter-period waves covering most parts of the Caribbean Sea during +SAM–El Niño, whereas only a very small area at the far end of its eastern portion experiences shorter-period waves during SAM–neutral–El Niño. The results obtained for the Caribbean Sea, once again, stress the importance of distinguishing between La Niña and El Niño when analysing wave anomalies during periods of active SAM and ENSO. As reported by Klein et al. (1999) and corroborated by the wind composites of Fig. 1, the atmospheric circulation over the South China Sea during El Niño opposes the mean austral summertime north-easterly flow, while during La Niña, the mean flow is enhanced. These wind anomalies maintain their sign under an active SAM background. Nevertheless, SAM-related atmospheric conditions can modulate the intensity of ENSO-related winds (Fig. 1) and, hence, the magnitude of waves in the South China Sea (Fig. 2), where larger waves are expected during La Niña (Zhu et al. 2015) and smaller waves during El Niño. The strengthening of north-easterly winds during combinations of −SAM and +SAM with La Niña (Fig. 1), relative to periods of SAM–neutral–La Niña, causes larger waves in the South China Sea northern half (Fig. 2). In combinations with El Niño, waves get even smaller during −SAM, when compared to SAM–neutral

periods, and become statistically non-significant in most areas of the South China Sea during +SAM, except in the southern portion.

4 Summary and conclusions

Understanding the differences in ocean wave conditions among the various coincident climate patterns phases is essential to protect vulnerable coastal and offshore infrastructures. We selected two climate patterns that have far-reaching-associated effects on the atmosphere and ocean, SAM and ENSO, and examined changes in ocean wave conditions during phase combinations between them. The examination was carried out by compositing daily anomalies in H_s, T_p, and surface winds during the austral summer over the period 1979–2018.

Despite tropic–tropic and tropic–extratropic teleconnections causing wind and wave anomalies across all ocean basins during the different SAM–ENSO phase combinations, the composites showed the dominance of these climate patterns in the areas where their respective signals are most evident. As a result of stronger mid- to high-latitude westerly winds blowing over the Southern Ocean, larger waves are observed in this ocean during combinations of +SAM with any ENSO phase. During combinations of −SAM with any ENSO phase, these winds are weaker, leading to smaller waves in that region. On the other hand, the larger waves off south-western Australia and in the southern South Atlantic, consistent with the northward displacement of storm tracks during −SAM, change significantly when −SAM is under an El Niño background. The waves in the southern South Atlantic increase even more and impact the southern African coast, whereas those off south-western Australia move further offshore and get smaller. The ENSO dominance manifests in the central and North Pacific, where waves increase during El Niño and decrease during La Niña, irrespective of the SAM phase. Peak wave periods behave somewhat different. Their composites revealed that the association of T_p with ENSO is generally stronger than with the SAM and that the strongest T_p anomalies in the Southern, Indian, and Pacific Oceans prevail during El Niño episodes, and the weakest T_p anomalies during La Niñas.

Two remarkable wave anomaly structures appear in the Pacific basin. Teleconnections associated with active SAM prevent the anomalously large waves expected along the California coast during El Niño events from occurring. In the Southern Hemisphere, wave anomalies around New Zealand, ascribed to El Niño and La Niña in past work (e.g., Gorman et al. 2003; Godoi et al. 2016), were found to be instead modulated by SAM phases in this study. These anomalies take place not only in the south-western Pacific Ocean, but also in the Tasman Sea and parts of the Southern Ocean.

Consistent with previous work (e.g., Marshall et al. 2018), larger waves in the North Atlantic demonstrate strong interhemispheric teleconnection to the SAM during its positive phase. Larger-than-usual waves impact the Bay of Biscay and surrounding coasts when +SAM and ENSO–neutral take place simultaneously. During El Niño episodes, positive wave anomalies in the North Atlantic are most critical along North America's coasts. Multi-hazard effects may arise from the co-occurrence of sea-level increases along the United States eastern seaboard (Domingues et al. 2018) with the larger and longer-period waves that impact that region during +SAM–El Niño. While such co-occurrence is likely to exacerbate coastal infrastructure damage, the waves experienced along the United States eastern seaboard when SAM–neutral and La Niña combine may help alleviate multi-hazard effects, since these waves are smaller than those that typically approach that region.

Changes in wave conditions are not limited to Ocean basins; semi-enclosed seas also experience marked variability due to SAM–ENSO interactions. Wave anomalies of opposite signs in the Caribbean Sea during periods in which +SAM combines with opposite ENSO phases are an example of the importance of distinguishing between El Niño and La Niña when the SAM and ENSO share anomalous activity. Previous work that considered active ENSO phases, but did not distinguish them when analysing relationships between wave anomalies and SAM phases (Marshall et al. 2018), could not identify these opposite anomalies in the Caribbean Sea. In the South China Sea, wind conditions associated with active ENSO phases dominate the signs of H_s and T_p anomalies during SAM–ENSO phase combinations, while SAM-related conditions can modulate the intensity of such anomalies.

Although some wave anomaly structures are more likely to happen due to the trend toward more positive SAM phases (Thompson and Solomon 2002; Marshall 2003), to the apparent changes in ENSO "flavour" (Ashok and Yamagata 2009; Freund et al. 2019), and the potential changes in ENSO frequency and magnitude (Cai et al. 2014, 2015), future climatic changes are still unclear (Yang et al. 2018). Whether these wave anomaly structures will hold or the extent to what they will change can only be determined through continuous climate monitoring. In spite of that, the wave composites presented here provide planners with valuable information on potential areas for wave disaster during SAM–ENSO phase combinations.

The chaotic nature of the ocean–atmosphere coupled system does not allow us to disregard the potential contribution to our results of wave conditions related to patterns other than those analysed here. Nevertheless, our findings demonstrate that assessing relationships between wave conditions and multiple concurrent climate patterns should be part of the broad scope of wave-related studies. We hope

these findings encourage similar investigations at regional and local scales considering other variables that can also impact the coast significantly, as, for instance, sea-level variability. These investigations will benefit coastal communities by assisting them in dealing better with multi-hazard effects.

Acknowledgements This research has been funded by the Brazilian National Council for Scientific and Technological Development (CNPq) (Grant number 153284/2018-8). The authors are thankful to the reviewers of this article, whose comments improved its earlier version, and also to the Australian Bureau of Meteorology, CSIRO, and NOAA for data provision.

References

Alexander MA, Bladé I, Newman M, Lanzante JR, Lau N, Scott JD (2002) The Atmospheric Bridge: the influence of ENSO teleconnections on air–sea interaction over the global oceans. J Clim 15(16):2205–2231. https://doi.org/10.1175/1520-0442(2002)015<2205:TABTIO>2.0.CO;2

Ardhuin F, Rogers E, Babanin AV, Filipot J-F, Magne R, Roland A, van der Westhuysen A, Queffeulou P, Lefevre J-M, Aouf L, Collard F (2010) Semiempirical dissipation source functions for ocean waves. Part I: definition, calibration, and validation. J Phys Oceanogr 40(9):1917–1941. https://doi.org/10.1175/2010jpo4324.1

Ashok K, Yamagata T (2009) The El Niño with a difference. Nature 461:481–484. https://doi.org/10.1038/461481a

Barnard PL, Short AD, Harley MD, Splinter KD, Vitousek S, Turner IL, Allan J, Banno M, Bryan KR, Doria A, Hansen JE, Kato S, Kuriyama Y, Randall-Goodwin E, Ruggiero P, Walker IJ, Heathfield DK (2015) Coastal vulnerability across the Pacific dominated by El Niño/Southern Oscillation. Nat Geosci 8:801–807. https://doi.org/10.1038/NGEO2539

Barnard PL, Hoover D, Hubbard DM, Snyder A, Ludka BC, Allan J, Kaminsky GM, Ruggiero P, Gallien TW, Gabel L, McCandless D, Weiner HM, Cohn N, Anderson DL, Serafin KA (2017) Extreme oceanographic forcing and coastal response due to the 2015–2016 El Niño. Nat Commun 8:14365. https://doi.org/10.1038/ncomms14365

Bjerknes J (1969) Atmospheric teleconnections from the equatorial Pacific. Mon Weather Rev 97(3):163–172. https://doi.org/10.1175/1520-0493(1969)097%3c0163:ATFTEP%3e2.3.CO;2

Bosserelle C, Pattiaratchi C, Haigh I (2012) Inter-annual variability and longer-term changes in the wave climate of Western Australia between 1970 and 2009. Ocean Dyn 62(1):63–76. https://doi.org/10.1007/s10236-011-0487-3

Bretherton CS, Widmann M, Dymnikov VP, Wallace JM, Bladé I (1999) The effective number of spatial degrees of freedom of a time-varying field. J Clim 12(7):1990–2009. https://doi.org/10.1175/1520-0442(1999)012%3c1990:TENOSD%3e2.0.CO;2

Cai W, van Rensch P, Cowan T (2011a) Teleconnection pathways of ENSO and the IOD and the mechanisms for impacts on Australian rainfall. J Clim 24:3910–3923. https://doi.org/10.1175/2011JCLI4129.1

Cai W, Sullivan A, Cowan T (2011b) Interactions of ENSO, the IOD, and the SAM in CMIP3 models. J Clim 24:1688–1704. https://doi.org/10.1175/2010JCLI3744.1

Cai W, Borlace S, Lengaigne M, van Rensch P, Collins M, Vecchi G, Timmermann A, Santoso A, McPhaden MJ, Wu L, England MH, Wang G, Guilyardi E, Jin F-F (2014) Increasing frequency of extreme El Niño events due to greenhouse warming. Nat Clim Change 4:111–116. https://doi.org/10.1038/nclimate2100

Cai W, Wang G, Santoso A, McPhaden MJ, Wu L, Jin F, Timmermann A, Collins M, Vecchi G, Lengaigne M, England MH, Dommenget D, Takahashi K, Guilyardi E (2015) Increased frequency of extreme La Niña events under greenhouse warming. Nat Clim Change 5:132–137. https://doi.org/10.1038/nclimate2492

Cane MA (2005) The evolution of El Niño, past and future. Earth Planet Sci Lett 230(3):227–240. https://doi.org/10.1016/j.epsl.2004.12.003

Carleton AM (2003) Atmospheric teleconnections involving the Southern Ocean. J Geophys Res 108(C4):8080. https://doi.org/10.1029/2000JC000379

Carvalho LMV, Jones C, Ambrizzi T (2005) Opposite phases of the Antarctic Oscillation and relationships with intraseasonal to interannual activity in the tropics during the austral summer. J Clim 18:702–718. https://doi.org/10.1175/JCLI-3284.1

Chase TN, Pielke R Sr, Avissar R (2006) Teleconnections in the Earth system. In: Anderson MG (ed) Encyclopedia of hydrological sciences. Wiley, New York. https://doi.org/10.1002/0470848944.hsa190

Chawla A, Spindler DM, Tolman HL (2013) Validation of a thirty year wave hindcast using the Climate Forecast System Reanalysis winds. Ocean Model 70:189–206. https://doi.org/10.1016/j.ocemod.2012.07.005

Chen G, Chapron B, Ezraty R, Vandemark D (2002) A global view of swell and wind sea climate in the ocean by satellite altimeter and scatterometer. J Atmos Ocean Technol 19:1849–1859. https://doi.org/10.1175/1520-0426(2002)019%3c1849:AGVOSA%3e2.0.CO;2

Colberg F, Reason CJC, Rodgers K (2004) South Atlantic response to El Niño–Southern Oscillation induced climate variability in an ocean general circulation model. J Geophys Res 109:C12015. https://doi.org/10.1029/2004JC002301

Collins M, An S-I, Cai W, Ganachaud A, Guilyardi E, Jin F-F, Jochum M, Lengaigne M, Power S, Timmermann A, Vecchi G, Wittenberg A (2010) The impact of global warming on the tropical Pacific Ocean and El Niño. Nat Geosci 3:391–397. https://doi.org/10.1038/NGEO868

Dare RA, Davidson NE (2004) Characteristics of tropical cyclones in the Australian region. Mon Weather Rev 132:3049–3065. https://doi.org/10.1175/MWR2834.1

Ding Q, Steig EJ, Battisti DS, Wallace JM (2012) Influence of the tropics on the Southern Annular Mode. J Clim 25:6330–6348. https://doi.org/10.1175/JCLI-D-11-00523.1

Ding H, Greatbatch RJ, Gollan G (2014) Tropical influence independent of ENSO on the austral summer Southern Annular Mode. Geophys Res Lett 41:3643–3648. https://doi.org/10.1002/2014GL059987

Domingues R, Goni G, Baringer M, Volkov D (2018) What caused the accelerated sea level changes along the U.S. East Coast during 2010–2015? Geophys Res Lett 45:13367–13376. https://doi.org/10.1029/2018gl081183

Durrant T, Hemer M, Trenham C, Greenslade D (2013a) CAWCR Wave Hindcast 1979–2010. v8. CSIRO. Service Collection. https://doi.org/10.4225/08/523168703dcc5

Durrant T, Hemer M, Trenham C, Greenslade D (2013b) CAWCR wave hindcast extension Jan 2011–May 2013. v5. CSIRO. Service Collection. https://doi.org/10.4225/08/52817e2858340

Durrant T, Greenslade D, Hemer M, Trenham C (2014) A global wave hindcast focussed on the Central and South Pacific. CAWCR Technical Report 70

Feldstein SB, Franzke CLE (2017) Atmospheric teleconnection patterns. In: Franzke C, O'Kane T (eds) Nonlinear and stochastic

climate dynamics. Cambridge University Press, Cambridge, pp 54–104. https://doi.org/10.1017/9781316339251.004
Fogt RL, Bromwich DH (2006) Decadal variability of the ENSO teleconnection to the high-latitude South Pacific governed by coupling with the Southern Annular Mode. J Clim 19:979–997. https://doi.org/10.1175/JCLI3671.1
Fogt RL, Perlwitz J, Monaghan AJ, Bromwich DH, Jones JM, Marshall GJ (2009) Historical SAM variability. Part II: twentieth-century variability and trends from reconstructions, observations, and the IPCC AR4 models. J Clim 22:5346–5365. https://doi.org/10.1175/2009JCLI2786.1
Fogt RL, Bromwich DH, Hines KM (2011) Understanding the SAM influence on the South Pacific ENSO teleconnection. Clim Dyn 36:1555–1576. https://doi.org/10.1007/s00382-010-0905-0
Freund MB, Henley BJ, Karoly DJ, McGregor HV, Abram NJ, Dommenget D (2019) Higher frequency of Central Pacific El Niño events in recent decades relative to past centuries. Nat Geosci 12:450–455. https://doi.org/10.1038/s41561-019-0353-3
Gillett NP, Thompson DWJ (2003) Simulation of recent Southern Hemisphere climate change. Science 302(5643):273–275. https://doi.org/10.1126/science.1087440
Godoi VA, Bryan KR, Gorman RM (2016) Regional influence of climate patterns on the wave climate of the southwestern Pacific: the New Zealand region. J Geophys Res Oceans 121(6):4056–4076. https://doi.org/10.1002/2015jc011572
Godoi VA, Bryan KR, Gorman RM (2018) Storm wave clustering around New Zealand and its connection to climatic patterns. Int J Climatol 38(S1):e401–e417. https://doi.org/10.1002/joc.5380
Godoi VA, de Andrade FM, Bryan KR, Gorman RM (2019) Regional-scale ocean wave variability associated with El Niño–Southern Oscillation-Madden-Julian Oscillation combined activity. Int J Climatol 39:483–494. https://doi.org/10.1002/joc.5823
Godoi VA, de Andrade FM, Durrant TH, Torres Júnior AR (2020) What happens to the ocean surface gravity waves when ENSO and MJO phases combine during the extended boreal winter? Clim Dyn 54:1407–1424. https://doi.org/10.1007/s00382-019-05065-9
Gong D, Wang S (1999) Definition of Antarctic Oscillation index. Geophys Res Lett 26(4):459–462. https://doi.org/10.1029/1999GL900003
Goodwin ID (2005) A mid-shelf, mean wave direction climatology for southeastern Australia, and its relationship to the El Niño—Southern Oscillation since 1878 A.D. Int J Climatol 25:1715–1729. https://doi.org/10.1002/joc.1207
Gorman RM, Bryan KR, Laing AK (2003) Wave hindcast for the New Zealand region: deep-water wave climate. NZ J Mar Freshw Res 37(3):589–612. https://doi.org/10.1080/00288330.2003.9517191
Grimm AM, Ambrizzi T (2009) Teleconnections into South America from the tropics and extratropics on interannual and intraseasonal timescales. In: Vimeux F, Sylvestre F, Khodri M (eds) Past climate variability in South America and surrounding regions Developments in paleoenvironmental research. Springer, Dordrecht, pp 159–191. https://doi.org/10.1007/978-90-481-2672-9_7
Harley MD, Turner IL, Short AD, Ranasinghe R (2010) Interannual variability and controls of the Sydney wave climate. Int J Climatol 30(9):1322–1335. https://doi.org/10.1002/joc.1962
Hemer MA (2010) Historical trends in Southern Ocean storminess: long-term variability of extreme wave heights at Cape Sorell, Tasmania. Geophys Res Lett 37:L18601. https://doi.org/10.1029/2010GL044595
Hemer MA, Church JA, Hunter JR (2010) Variability and trends in the directional wave climate of the Southern Hemisphere. Int J Climatol 30(4):475–491. https://doi.org/10.1002/joc.1900
Hemer MA, Zieger S, Durrant T, O'Grady J, Hoeke RK, McInnes KL, Rosebrock U (2017) A revised assessment of Australia's national wave energy resource. Renew Energy 114(A):85–107. https://doi.org/10.1016/j.renene.2016.08.039
Ho M, Kiem AS, Verdon-Kidd DC (2012) The Southern Annular Mode: a comparison of indices. Hydrol Earth Syst Sci 16:967–982. https://doi.org/10.5194/hess-16-967-2012
Hoskins BJ, Yang G-Y (2000) The equatorial response to higher-latitude forcing. J Atmos Sci 57(9):1197–1213. https://doi.org/10.1175/1520-0469(2000)057%3c1197:TERTHL%3e2.0.CO;2
Hurwits MM, Newman PA, Oman LD, Molod AM (2011) Response of the Antarctic stratosphere to two types of El Niño vvents. J Atmos Sci 68:812–822. https://doi.org/10.1175/2011JAS3606.1
Izaguirre C, Méndez FJ, Menéndez M, Losada IJ (2011) Global extreme wave height variability based on satellite data. Geophys Res Lett 38(10):L10607. https://doi.org/10.1029/2011GL047302
Karoly DJ (1989) Southern Hemisphere circulation features associated with El Niño–Southern Oscillation events. J Clim 2(11):1239–1252. https://doi.org/10.1175/1520-0442(1989)002%3c1239:SHCFAW%3e2.0.CO;2
Klein SA, Soden BJ, Lau N-C (1999) Remote sea surface temperature variations during ENSO: evidence for a tropical atmospheric bridge. J Clim 12:917–932. https://doi.org/10.1175/1520-0442(1999)012%3c0917:RSSTVD%3e2.0.CO;2
Kumar P, Kaur S, Weller E, Min S-K (2019) Influence of natural climate variability on the extreme ocean surface wave heights over the Indian Ocean. J Geophys Res Oceans 124:6176–6199. https://doi.org/10.1029/2019jc015391
L'Heureux ML, Thompson DWJ (2006) Observed relationships between the El Niño–Southern Oscillation and the extratropical zonal-mean circulation. J Clim 19:276–287. https://doi.org/10.1175/JCLI3617.1
L'Heureux ML, Lee S, Lyon B (2013) Recent multidecadal strengthening of the Walker circulation across the tropical Pacific. Nat Clim Change 3:571–576. https://doi.org/10.1038/NCLIMATE1840
Lim E-P, Hendon HH, Rashid H (2013) Seasonal predictability of the Southern Annular Mode due to its association with ENSO. J Clim 23:8037–8054. https://doi.org/10.1175/JCLI-D-13-00006.1
Limpasuvan V, Hartmann DL (1999) Eddies and the annular modes of climate variability. Geophys Res Lett 26(20):3133–3136. https://doi.org/10.1029/1999GL010478
Liu Z, Alexander M (2007) Atmospheric bridge, oceanic tunnel, and global climatic teleconnections. Rev Geophys 45:RG2005. https://doi.org/10.1029/2005rg000172
Liu T, Li J, Zheng F (2015) Influence of the boreal autumn Southern Annular Mode on winter precipitation over land in the Northern Hemisphere. J Clim 28:8825–8839. https://doi.org/10.1175/JCLI-D-14-00704.1
Liu T, Li J, Li YJ, Zhao S, Zheng F, Zheng J, Yao Z (2018) Influence of the May Southern Annular Mode on the South China Sea summer monsoon. Clim Dyn 51(11–12):4095–4107. https://doi.org/10.1007/s00382-017-3753-3
MacRitchie K, Roundy PE (2016) The two-way relationship between the Madden-Julian Oscillation and anticyclonic wave breaking. Q J R Meteorol Soc 142:2159–2167. https://doi.org/10.1002/qj.2809
Madden RA, Julian PR (1971) Detection of a 40–50 day oscillation in the zonal wind in the tropical Pacific. J Atmos Sci 28:702–708. https://doi.org/10.1175/1520-0469(1971)028%3c0702:DOADOI%3e2.0.CO;2
Madden RA, Julian PR (1972) Description of global-scale circulation cells in the tropics with a 40–50 day period. J Atmos Sci 29:1109–1123. https://doi.org/10.1175/1520-0469(1972)029%3c1109:DOGSCC%3e2.0.CO;2
Madden RA, Julian PR (1994) Observations of the 40–50-day tropical oscillation—a review. Mon Weather Rev 122:814–837.

https://doi.org/10.1175/1520-0493(1994)122%3c0814:OOTDTO%3e2.0.CO;2
Mamalakis A, Yu J-Y, Randerson JT, AghaKouchak A, Foufoula-Georgiou E (2018) A new interhemispheric teleconnection increases predictability of winter precipitation in southwestern US. Nat Commun 9:2332. https://doi.org/10.1038/s41467-018-04722-7
Marshall GJ (2003) Trends in the Southern Annular Mode from observations and reanalyses. J Clim 16(24):4134–4143. https://doi.org/10.1175/1520-0442(2003)016%3c4134:TITSAM%3e2.0.CO;2
Marshall AG, Hemer MA, Hendon HH, McInnes KL (2018) Southern annular mode impacts on global ocean surface waves. Ocean Model 129:58–74. https://doi.org/10.1016/j.ocemod.2018.07.007
McBride JL, Keenan TD (1982) Climatology of tropical cyclone genesis in the Australian region. J Climatol 2(1):13–33. https://doi.org/10.1002/joc.3370020103
Mechoso CR, Hartmann DL, Farrara JD (1985) Climatology and interannual variability of wave mean-flow interaction in the Southern. Hemisphere 42(20):2189–2206. https://doi.org/10.1175/1520-0469(1985)042%3c2189:CAIVOW%3e2.0.CO;2
Mo KC (2000) Relationships between low-frequency variability in the Southern Hemisphere and sea surface temperature anomalies. J Clim 13:3599–3610. https://doi.org/10.1175/1520-0442(2000)013%3c3599:RBLFVI%3e2.0.CO;2
Mo KC, Paegle JN (2001) The Pacific-South American modes and their downstream effects. Int J Climatol 21(10):1211–1229. https://doi.org/10.1002/joc.685
Munk WH, Snodgrass FE (1957) Measurements of southern swell at Guadalupe Island. Deep Sea Res 4:272–286. https://doi.org/10.1016/0146-6313(56)90061-2
Munk WH, Miller GR, Snodgrass FE, Barber NF (1963) Directional recording of swell from distant storms. Philos Trans R Soc A 255:505–584. https://doi.org/10.1098/rsta.1963.0011
Nan S, Li J (2003) The relationship between the summer precipitation in the Yangtze River valley and the boreal spring Southern Hemisphere annular mode. Geophys Res Lett 30(24):2266. https://doi.org/10.1029/2003GL018381
Neelin JD, Battisti DS, Hirst AC, Jin F-F, Wakata Y, Yamagata T, Zebiak SE (1998) ENSO theory. J Geophys Res Oceans 103(C7):14261–14290. https://doi.org/10.1029/97JC03424
Philander SGH (1983) El Niño Southern Oscillation phenomena. Nature 302:295–301. https://doi.org/10.1038/302295a0
Reguero BG, Losada IJ, Méndez FJ (2015) A global wave power resource and its seasonal, interannual and long-term variability. Appl Energy 148:366–380. https://doi.org/10.1016/j.apenergy.2015.03.114
Rogers JC, van Loon H (1982) Spatial variability of sea level pressure and 500 mb height anomalies over the Southern Hemisphere. Mon Weather Rev 110:1375–1392. https://doi.org/10.1175/1520-0493(1982)110%3c1375:SVOSLP%3e2.0.CO;2
Rudeva I, Simmonds I (2015) Variability and trends of global atmospheric frontal activity and links with large-scale modes of variability. J Clim 28:3311–3330. https://doi.org/10.1175/JCLI-D-14-00458.1
Saha S, Moorthi S, Pan H, Wu X, Wang J, Nadiga S, Tripp P, Kistler R, Wollen J, Behringer D, Liu H, Stokes D, Grumbine R, Gayno G, Wang J, Hou Y, Chuang H, Juang HH, Sela J, Iredell M, Treadon R, Kleist D, Van Delst P, Keyser D, Derber J, Ek M, Meng J, Wei H, Yang R, Lord S, van den Dool H, Kumar A, Wang W, Long C, Chelliah M, Xue Y, Huang B, Schemm J, Ebisuzaki W, Lin R, Xie P, Chen M, Zhou S, Higgins W, Zou C, Liu Q, Chen Y, Han Y, Cucurull L, Reynolds R, Rutledge G, Goldberg M (2010) The NCEP climate forecast system reanalysis. Bull Am Meteorol Soc 91:1015–1057. https://doi.org/10.1175/2010BAMS3001.1
Saha S, Moorthi S, Wu X, Wang J, Nadiga S, Tripp P, Behringer D, Hou Y-T, Chuang H, Iredell M, Ek M, Meng J, Yang R, Mendez MP, van den Dool H, Zhang Q, Wang W, Chen M, Becker E (2014) The NCEP Climate Forecast System version 2. J Clim 27:2185–2208. https://doi.org/10.1175/JCLI-D-12-00823.1
Semedo A, Sušelj K, Rutgersson A, Sterl A (2011) A global view on the wind sea and swell climate and variability from ERA-40. J Clim 24:1461–1479. https://doi.org/10.1175/2010JCLI3718.1
Shimizu MH, Cavalcanti IFA (2011) Variability patterns of Rossby wave source. Clim Dyn 37:441–454. https://doi.org/10.1007/s00382-010-0841-z
Shimura T, Mori N, Mase H (2013) Ocean waves and teleconnection patterns in the Northern Hemisphere. J Clim 26:8654–8670. https://doi.org/10.1175/JCLI-D-12-00397.1
Simmonds I, King JC (2004) Global and hemispheric climate variations affecting the Southern Ocean. Antarct Sci 16(4):401–413. https://doi.org/10.1017/S0954102004002226
Snodgrass FE, Groves GW, Hasselmann KF, Miller GR, Munk WH, Powers WH (1966) Propagation of ocean swell across the pacific. Philos Trans R Soc A 259:431–497
Stammerjohn SE, Martinson DG, Smith RC, Yuan X, Rind D (2008) Trends in Antarctic annual sea ice retreat and advance and their relation to El Niño–Southern Oscillation and Southern Annular Mode variability. J Geophys Res 113(C3):C03S90. https://doi.org/10.1029/2007jc004269
Stan C, Straus DM, Frederiksen JS, Lin H, Maloney ED, Schumacher C (2017) Review of tropical–extratropical teleconnections on intraseasonal time scales. Rev Geophys 55(4):902–937. https://doi.org/10.1002/2016RG000538
Sterl A, Caires S (2005) Climatology, variability and extrema of ocean waves: the Web-based KNMI/ERA-40 wave atlas. Int J Climatol 25:963–977. https://doi.org/10.1002/joc.1175
Stopa JE (2018) Wind forcing calibration and wave hindcast comparison using multiple reanalysis and merged satellite wind datasets. Ocean Model 127:55–69. https://doi.org/10.1016/j.ocemod.2018.04.008
Stopa JE, Cheung KF (2014) Periodicity and patterns of ocean wind and wave climate. J Geophys Res Oceans 119:5563–5584. https://doi.org/10.1002/2013JC009729
Stopa JE, Cheung KF, Tolman HL, Chawla A (2013) Patterns and cycles in the Climate Forecast System Reanalysis wind and wave data. Ocean Model 70:207–220. https://doi.org/10.1016/j.ocemod.2012.10.005
Student (1908) The probable error of a mean. Biometrika 6(1):1–25. https://doi.org/10.2307/2331554
Sun J-Q (2010) Possible impact of the boreal spring Antarctic Oscillation on the North American summer monsoon. Atmos Ocean Sci Lett 3(4):232–236. https://doi.org/10.1080/16742834.2010.11446870
Sun J-Q, Wang H, Yuan W (2010) Linkage of the boreal spring Antarctic Oscillation to the West African summer monsoon. J Meteorol Soc Jpn 88(1):15–28. https://doi.org/10.2151/jmsj.2010-102
Thompson DWJ, Solomon S (2002) Interpretation of recent Southern Hemisphere climate change. Science 296(5569):895–899. https://doi.org/10.1126/science.1069270
Thompson DWJ, Wallace JM (2000) Annular modes in the extratropical circulation. Part I: month-to-month variability. J Clim 13:1000–1016. https://doi.org/10.1175/1520-0442(2000)013%3c1000:AMITEC%3e2.0.CO;2
Tolman HL (1991) A third-generation model for wind waves on slowly varying, unsteady, and inhomogeneous depths and currents. J Phys Oceanogr 21:782–797. https://doi.org/10.1175/1520-0485(1991)021%3c0782:ATGMFW%3e2.0.CO;2
Tolman HL (2014) User manual and system documentation of WAVEWATCH III™ version 4.18. Technical Note 316, NOAA/NWS/NCEP/MMAB

Trenberth KE, Hurrell JW (1994) Decadal atmosphere-ocean variations in the Pacific. Clim Dyn 9(6):303–319. https://doi.org/10.1007/BF00204745

Turner J (2004) The El Niño–Southern Oscillation and Antarctica. Int J Climatol 24:1–31. https://doi.org/10.1002/joc.965

Veitch J, Rautenbach C, Hermes J, Reason C (2019) The Cape Point wave record, extreme events and the role of large-scale modes of climate variability. J Mar Syst 198:103185. https://doi.org/10.1016/j.jmarsys.2019.103185

Vera CS, Osman M (2018) Activity of the Southern Annular Mode during 2015–2016 El Niño event and its impact on Southern Hemisphere climate anomalies. Int J Climatol 38(S1):e1288–e1295. https://doi.org/10.1002/joc.5419

Vousdoukas MI, Mentaschi L, Voukouvalas E, Verlaan M, Feyen L (2017) Extreme sea levels on the rise along Europe's coasts. Earth's Future. https://doi.org/10.1002/2016EF000505

Walker GT, Bliss EW (1932) World weather V. Mem R Meteorol Soc 4(36):53–84

Walker GT, Bliss EW (1937) World weather VI. Mem R Meteorol Soc 4(39):119–139

Wang G, Cai W (2013) Climate-change impact on the 20th-century relationship between the Southern Annular Mode and global mean temperature. Sci Rep 3:1–6. https://doi.org/10.1038/srep02039

Wilks DS (2006) Statistical methods in the atmospheric sciences, 3rd edn. Academic Press, London. https://doi.org/10.1016/s0074-6142(06)80036-7

Wu Z, Li J, Wang B, Liu X (2009) Can the Southern Hemisphere annular mode affect China winter monsoon? J Geophys Res 114:D11107. https://doi.org/10.1029/2008JD011501

Yang S, Li Z, Yu J-Y, Hu X, Dong W, He S (2018) El Niño–Southern Oscillation and its impact in the changing climate. Natl Sci Rev 5(6):840–857. https://doi.org/10.1093/nsr/nwy046

Young IR (1999) Seasonal variability of the global ocean wind and wave climate. Int J Climatol 19(9):931–950. https://doi.org/10.1002/(SICI)1097-0088(199907)19:9%3c931:AID-JOC412%3e3.0.CO;2-O

Yu J-Y, Paek H, Saltzman ES (2015) The early 1990s change in ENSO–PSA–SAM relationships and its impact on Southern Hemisphere climate. J Clim 28:9393–9408. https://doi.org/10.1175/JCLI-D-15-0335.1

Zhu G, Lin W, Zhao S, Cao Y (2015) Spatial and temporal variation characteristics of ocean waves in the South China Sea during the boreal winter. Acta Oceanol Sin 34(1):23–28. https://doi.org/10.1007/s13131-015-0592-0